The signature of shear-wave splitting: Theory and observations on heavy oil data

Richard Bale, Tobin Marchand, and Keith Wilkinson, Key Seismic Solutions
Kurtis Wikel, Petrobank Energy and Resources
Robert Kendall, Tesla Exploration Ltd.

The use of shear-wave splitting analysis as a tool for fracture analysis is well established. In this article, we discuss the analysis of shear-wave splitting in a relatively new context—shallow heavy oil plays where we believe stress is the dominant cause of the shear-wave splitting, rather than macroscale fracturing. There is clear laboratory evidence in the literature for shear-wave splitting caused by differential stress, which we believe supports this viewpoint. We are particularly interested in the use of shear-wave splitting technology for monitoring reservoir stress changes which correlate with thermal production for heavy oil reservoirs. This article also takes a fresh look at some well-established characteristics of split shear waves as they appear in wide-azimuth multicomponent data, and in particular the relative merits of the radial and transverse amplitude signatures. We describe a recently developed method which combines both radial and transverse analysis to improve the effective azimuthal coverage. This approach is beneficial when the survey has been coarsely acquired, as we demonstrate on a heavy oil example. The article concludes with a case study at Kerrobert, a reservoir in the Canadian heavy oil region where thermal recovery methods are in use, and where shear-wave splitting is being utilized to help characterize the resulting stress changes in the reservoir.

Introduction

There is increasing interest in using PS data from multicomponent surveys over heavy oil or oil sands reservoirs for characterizing stress—particularly in the overburden and as it relates to cap-rock integrity analysis. An example of time-lapse stress analysis from PS data for the overburden is described in some detail in Wikel et al. (2012), for enhanced oil recovery (EOR) using THAI thermal production. For details of the THAI method, we refer the interested reader to that paper. The PS processing for stress mapping at another heavy oil THAI project was subsequently described in more detail in Bale et al. (2012). Our premise is that the changes in stress associated with production activity in thermal EOR processes give rise to anomalies in the amount of shear-wave splitting. Hence, accurate measurement of shear-wave splitting attributes, namely S1 azimuth and time delay, is of paramount importance for monitoring all thermal recovery methods.

Given the high noise levels associated with land data, it is often a challenge to detect and measure the subtle signal associated with shear-wave splitting over heavy oil reservoirs. This is exacerbated for shallow data where fold and azimuth distributions are restricted. In particular the signal present on the transverse component—which is important in the analysis for shear-wave splitting—can sometimes be weak compared to noise, and must be enhanced using "superbins." On the other hand, signal-to-noise on the radial component is usually much higher. We will analyze these differences, to understand the relative information content of radial and transverse responses to splitting, and how we may utilize both. Before we turn to that question, we first examine the rock physical

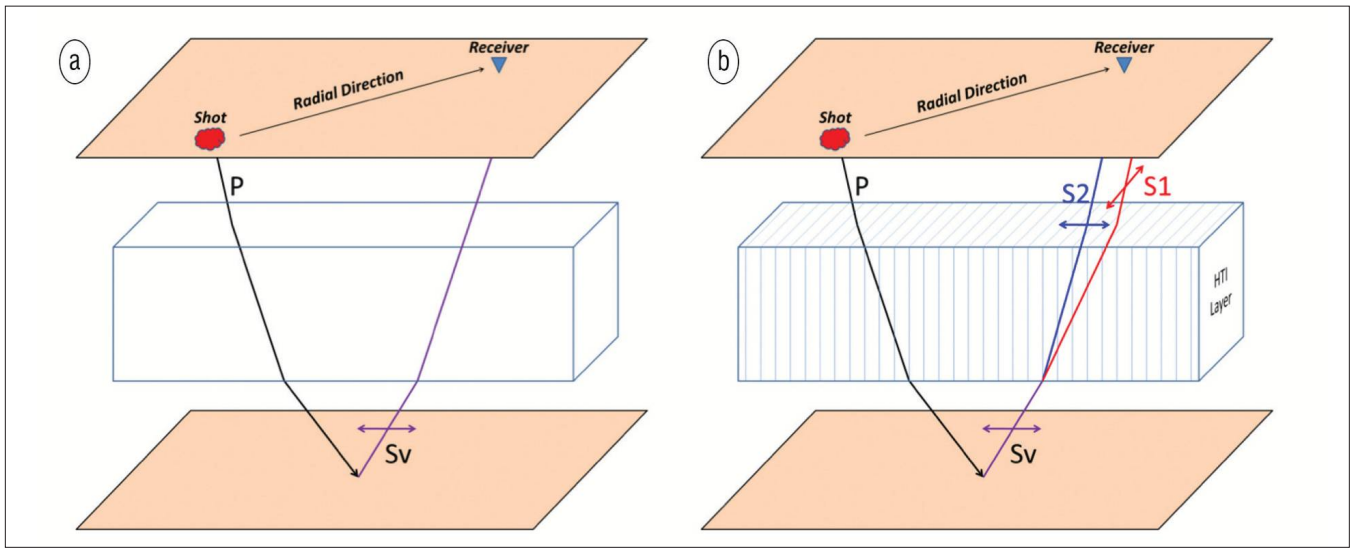

Figure 1. *Diagram illustrating the concept of converted-wave splitting in an HTI media. Without HTI anisotropy, the wave propagates without splitting (a). With HTI anisotropy the converted wave splits into two modes, labelled S1 and S2 (b). The layering can be thought of as vertical fracturing or the regional direction of maximum horizontal stress in the absence of fractures (from Wikel et al., 2012).*

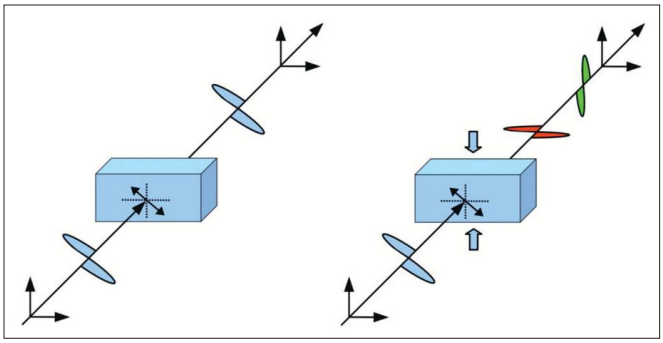

Figure 2. *Configuration for ultrasonic shear-wave experiment described in Dillen (2000, Figure 5.3). The Colton sandstone block is probed with a shear wave generated by a transducer oriented diagonally to the face. The situation with equal stresses applied in all directions is illustrated on the left, and no splitting is observed. The situation with a differential stress between the two directions transverse to the propagation direction is shown on the right. In the latter case, the higher stress direction (vertical) is the direction of the faster shear wave.*

basis for our observations of stress-related splitting in unconsolidated sediments and heavy oil reservoirs.

The rock physics of shear-wave splitting from stress anisotropy

Historically, shear-wave splitting analysis has focussed on the detection of fracturing in the subsurface, typically assumed to be represented as an HTI medium (Figure 1) (e.g., Thomsen et al., 1999; Gumble and Gaiser, 2006; Simmons, 2009). An HTI medium is one with a single horizontal axis of symmetry: for example, a single set of vertical fractures. Near-surface splitting analysis, and correction by layer stripping, was often regarded as simply a preliminary step both to improve the PS imaging of deeper structure and to facilitate the deeper fracture analysis. However, recently, especially for shallow heavy oil reservoirs, attention has been shifting toward the anisotropy analysis of the near surface itself (e.g., Whale et al., 2009).

Analysis in the near surface, and at other depths, where fracturing is unlikely to be the main source of anisotropy, has nonetheless shown clear indications of shear-wave splitting. This could be in the very near surface where unconsolidated sediments dominate the geology (Cary et al., 2010), or at deeper depths, where fracturing is known to be minimal to nonexistent from extensive oil sands exploration wells and core (Wikel et al., 2012). However, the mechanism whereby shear-wave splitting results from stress anisotropy is not widely appreciated. It is worth an overview, with an emphasis on rock physics, before we discuss shear-wave splitting analysis and processing in detail.

Sayers (2010) shows laboratory ultrasonic measurements of both isotropic confining stress variation and axial stress variation with constant radial stress (Figures 2 and 4, respectively, in chapter 4 of the text *Geophysics Under Stress: Geomechanical Applications of Seismic and Borehole Acoustic Waves* which accompanied Sayers' 2010 Distinguished Instructor Short Course). The shear-wave results from the second of these tests display variation based on both the propagation direction and polarization relative to the stress directions.

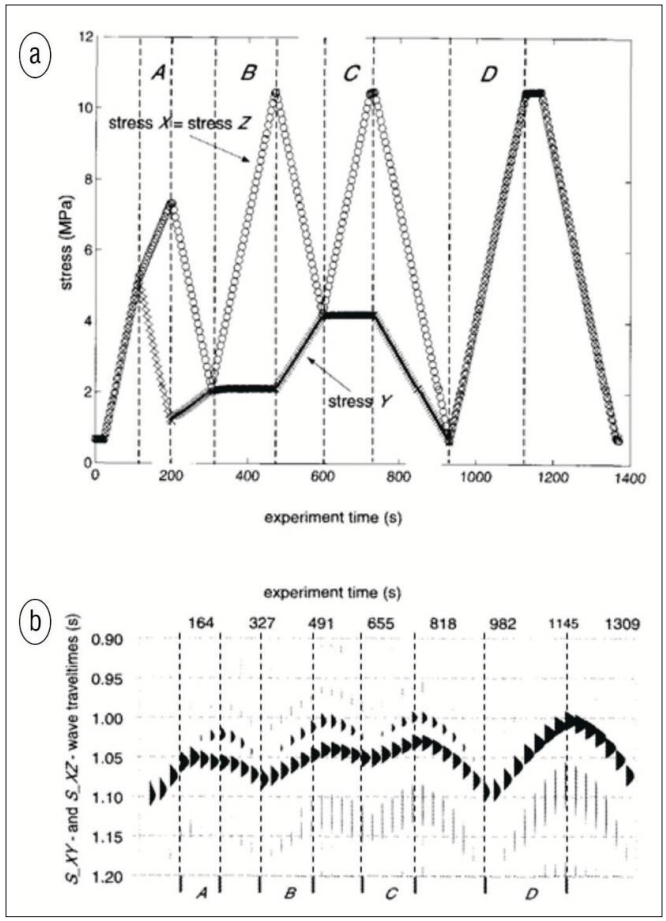

Figure 3. *(a) Variation of stress (load cycle ABCD) applied using triaxial pressure machine on a Colton sandstone. To preserve the intrinsic transverse isotropy of the sample, the stress in the x-direction is equal to the stress in the z-direction, whereas the y-direction stress is lower, except for cycle D, where all stresses are equal. (b) Shear-wave splitting recorded using diagonal transducers with wave propagating in the x-direction, as illustrated in Figure 2, during load cycle ABCD. Note the presence of splitting associated with differential stress (A, B, and C) and the absence of splitting when there is no differential stress (D). (Modified, with permission, from Figures 5.1 and 5.3 in Dillen.)*

Dillen (2000) shows that the phenomenon of shear-wave splitting occurs from stress anisotropy, observed on a triaxial ultrasonic stress test for a sample of Colton sandstone, an Eocene fluvial deposit in north-central Utah. The setup which Dillen describes for the shear-wave splitting test is illustrated in Figure 2. The S-wave transducers are placed on a face of the block, at a 45° diagonal orientation relative to the vertical axis. There are two situations during the test, one in which the variable stresses applied are all equal, and one in which the stresses in the two directions orthogonal to the wave propagation are not equal, with the vertical stress being higher. This leads to splitting as illustrated in Figure 2.

We reproduce two key figures from Dillen's thesis in Figure 3. Figure 3a shows the variation of stresses applied in *x*, *y* and *z* directions during experiment time. The *x* and *z* stresses are kept equal throughout, whereas in the first three stages (labelled A, B, and C) in the plot, the y stress is lower. During the fourth stage (D), all three stresses are equal. The recorded waveforms in Figure 3b result from a shear wave propagating

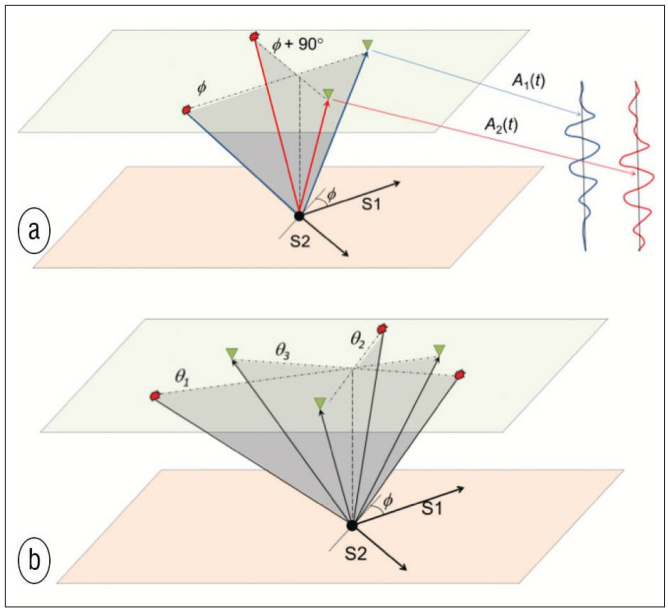

Figure 4. *Diagram illustrating the amplitude-dependence on azimuth for shear-wave splitting: (a) the responses measured for an ideal, two-azimuth geometry with an azimuth parallel to the fast shear (S1) direction giving a response* $A_1(t)$ *and an azimuth parallel to the slow shear (S2) direction giving a response* $A_2(t)$ *and (b) the actual geometry with multiple azimuths* θ_1, θ_2, *etc.*

parallel to the *x* axis, generated and recorded by the diagonal transducers on opposite *y*-*z* faces, as depicted in Figure 2. Note the clear emergence of splitting during the A, B, and C stages (when the stress in the *z* direction is higher than in the *y* direction), and the disappearance of splitting when the stresses are equal (stage D). This experiment is analogous (after the obvious 90° rotation of axes) to the surface seismic situation where we have propagation in the vertical direction and a differential stress between the two horizontal directions.

The stress effect is attributed to the creation of microcracks within the sample in the direction of maximum horizontal stress—i.e., faster velocities parallel to pore-scale microfracturing and slower velocities perpendicular (Sayers, 2010). It is easiest to view stress anisotropy from fracturing or from stress as a function of the same mechanism, albeit at different scales. The same mechanism operates at both macro (regional or formation) scale and micro (pore) scale in a conventional consolidated rock (in these cases consolidated sandstones). In the case of unconsolidated reservoirs, such as heavy oil and bitumen, the matrix is often poorly connected, or made up of the heavy oil or bitumen itself. It is possible that in EOR processes matrix reorganization occurs with recovery. This reorganization of the matrix could be the cause of shear-wave splitting—in addition to, or in concert with, stress anisotropy. However, this concept has not been tested on bitumen sands in the lab to our knowledge and warrants further investigation as a mechanism of splitting.

It is this S-wave polarization property that allows us to gauge stress anisotropy in the subsurface using shear-wave splitting from converted-wave data. Before describing a recently developed approach to measure shear-wave splitting on 3D land seismic, we will re-examine some aspects of the seismic signature associated with shear-wave splitting to get further insight into the problem.

The shear-wave splitting signature

A convenient domain for detection of shear-wave splitting, and analysis of the fast and slow directions or "principal axes", is after a rotation to radial and transverse directions. Radial refers to the direction aligned with the source receiver azimuth, and transverse is the direction perpendicular to radial, 90° clockwise in the convention adopted here. The radial and transverse data can be analyzed prestack or after partial stacking into azimuthal sectors. The analysis can also be applied after prestack migration provided that azimuthal information is retained, for example by using a common-offset vector (COV) or offset-vector tile (OVT) based migration.

In the absence of any azimuthal anisotropy, and assuming a layered medium, there will be no coherent signal present on the transverse component. Therefore, one preliminary indication that shear-wave splitting is present will be observable signal on the transverse component. It should be noted that signal can also arise on the transverse component for other reasons such as structure. The characteristic of splitting related signal is that it will have a 2θ periodicity, with polarity reversals every 90°, and this is generally not the case with other causes of transverse signal. So it is natural to find methods that search for this kind of periodic signal on the transverse data as an indication of probable anisotropy. A number of shear-wave splitting analysis methods are based on this (e.g. Li, 1998; Bale et al., 2005). Gaiser et al. (1997) describe a related approach based on converted-wave "Alford rotation."

With regard to the radial component, there is often observed an apparent sinusoidal time signature which also has 2θ periodicity. This is superficially similar to the corresponding velocity variation with azimuth (VVAZ) which is observed on pure P-wave data. However, we will see that there are important differences between these apparently similar manifestations.

Often the signal on the transverse is quite weak and is difficult to analyze in the presence of noise. The radial component, by contrast, typically has a high signal-to-noise ratio (SNR). In fact, when we observe higher SNR on transverse than on radial it is almost always an indication that there has been a mistake made in processing—typically in the definition of the rotation! So, given the higher SNR of the radial component, it is tempting to try and exploit this advantage, by using the radial for anisotropy analysis in preference to the transverse. But is this advantage real or illusory? Let's look more closely at the characteristics of both components.

We will be thinking, in general, about a converted wave of arbitrary azimuth which splits into two shear waves polarized parallel to the fast (S1) and slow (S2) directions, which we will refer to as the P-S1 and P-S2 modes respectively. In general the azimuth direction is not necessarily parallel to either S1 or S2.

Figure 4a illustrates an ideal but impractical situation where PS data are acquired with two azimuths, one parallel

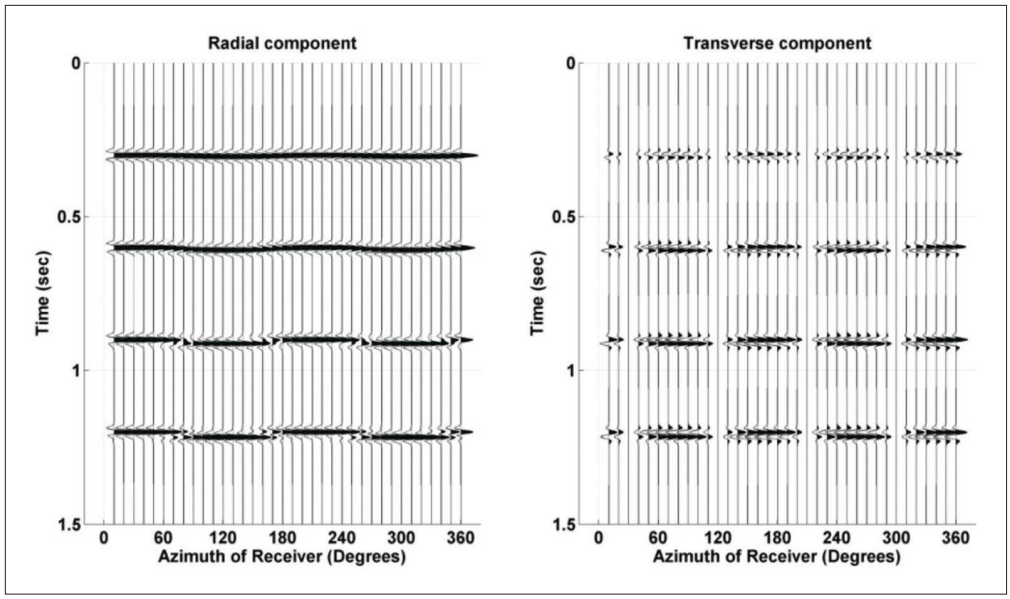

Figure 5. *Synthetic gather used to illustrate splitting amplitude effects. Radial component (left) and transverse component (right) displayed as a function of azimuth from shot to receiver. The S1 direction is 30° and the medium has a constant 2% velocity difference between S1 and S2.*

to the S1 direction and one parallel to the S2 direction. The response from these two source-receiver pairs are called $A_1(t)$ and $A_2(2)$ respectively. This is not possible in practice—quite apart from obvious acquisition limitations—because we do not know the directions of S1 and S2. Figure 4b illustrates the actual situation where we acquire several different azimuths (more than the three illustrated here in general) and none are aligned perfectly with S1 or S2. For the geometry of Figure 4b, we can write the amplitudes of the radial and transverse components in terms of the ideal measurements as

$$R(t,\theta_i) = A_1(t)\cos^2(\theta_i-\varphi) + A_2(t)\sin^2(\theta_i-\varphi) \quad (1a)$$

and

$$T(t,\theta_i) = [A_1(t) - A_2(t)]\sin(\theta_i-\varphi)\cos(\theta_i-\varphi) \quad (1b)$$

for an S1 direction φ, and N traces with radial directions θ_i.

These trigonometric terms are the cause of the observed periodicity behavior. They result from the projection of the initially radially oriented PS conversion onto either S1 or S2, in the Earth, followed by the subsequent projections back onto radial or transverse by the numerical rotation of the receiver in the computer.

What are we neglecting here? AVO effects are not included—so these equations need to be considered as applying to data with similar offsets, or some form of offset equalization must be applied. We are also making an assumption of near-vertical S-wave propagation. This assumption means that the first-order traveltimes of P-S1 and P-S2 are not azimuth dependent (recall that the azimuth is not the same necessarily as the polarization direction). This may seem confusing as we are considering azimuthal anisotropy. However, a characteristic of converted waves (and the important difference compared to P-wave VVAZ) is that there is a time difference between P-S1 and P-S2 modes even at zero offset, because S1 and S2 propagate vertically with different velocities, having different polarizations. Of course, strictly speaking there should be no amplitude at zero offset for PS, but the near-offset behavior can certainly be approximated to consist of S1 and S2 polarized waves which have constant, but different, velocities. As we move to larger offsets, this assumption becomes more suspect and there will be some azimuthal variation of both the P-wave leg and the individual S1 and S2 legs. However, observation suggests that the dominant effect in most cases of relevance to surface seismic recording is simply the time delay between S1 and S2. Indeed, a recent synthetic study by Liu et al. (2012) concluded that "the traveltime delay between the P-SV1 and P-SV2 wave is more significant than the azimuthal travel-time variation of both the P-SV1 and P-SV2 wave"—for a given offset.

Returning to the amplitude expressions for radial and transverse given in Equation 1, we can rewrite them as

$$R(t,\theta_i) = \bar{A}(t) + \Delta A(t)\cos[2(\theta_i-\varphi)] \quad (2a)$$

and

$$T(t,\theta_i) = \Delta A(t)\sin[2(\theta_i-\varphi)] \quad (2b)$$

where $\bar{A}(t) = \frac{1}{2}[A_1(t) + A_2(t)]$ and $\Delta A(t) = \frac{1}{2}[A_1(t) - A_2(t)]$, are simply the average and half difference of the ideal S1 and S2 responses, respectively.

By rewriting in this form we observe something interesting. The part of the radial component which is sensitive to azimuth (the second term in Equation 2a) is no stronger in amplitude than the transverse component, Equation 2b. The strong signal on the radial is due to the first term, $\bar{A}(t)$, which has no dependence on the fast direction φ. This suggests that, taken in isolation, the radial component has no advantage or disadvantage for estimation of φ, compared to the transverse. However, another interesting observation from Equation 2 is that radial and transverse have a different phase in their dependence on φ, so that one or the other may have higher signal levels than the other, for any given azimuth. This suggests that, for a well distributed set of azimuths, the combination of radial and transverse may have higher average SNR than either alone.

To illustrate these points, we have constructed a simple synthetic which consists of a constant medium with 2% difference between S1 and S2 velocities, and a constant S1 azimuth of 30° from N (Figure 5). Four equally spaced

reflections have been modeled, and the total amount of time delay between S1 and S2 is simply proportional to reflection time. Thus we can see the progressive change in the nature of the shear-wave splitting signature as the S1-S2 delay time increases.

Figure 6a shows the decomposition of the first reflection event into the azimuthally independent ($\bar{A}$) term and the azimuthally dependent term for the radial, and compares the latter with the azimuthal variation present in the transverse component. As predicted from Equation 2, the part which depends on φ, is of the same magnitude as, but different phase to, the transverse component. (For the synthetic case, this decomposition is possible by modeling, but in general it is a by-product of the azimuthal analysis we describe in the following section.)

How does the appearance of sinusoidal time variation on the radial come about? As can be seen in Figure 6a, this is actually a consequence of interference between the S1 and

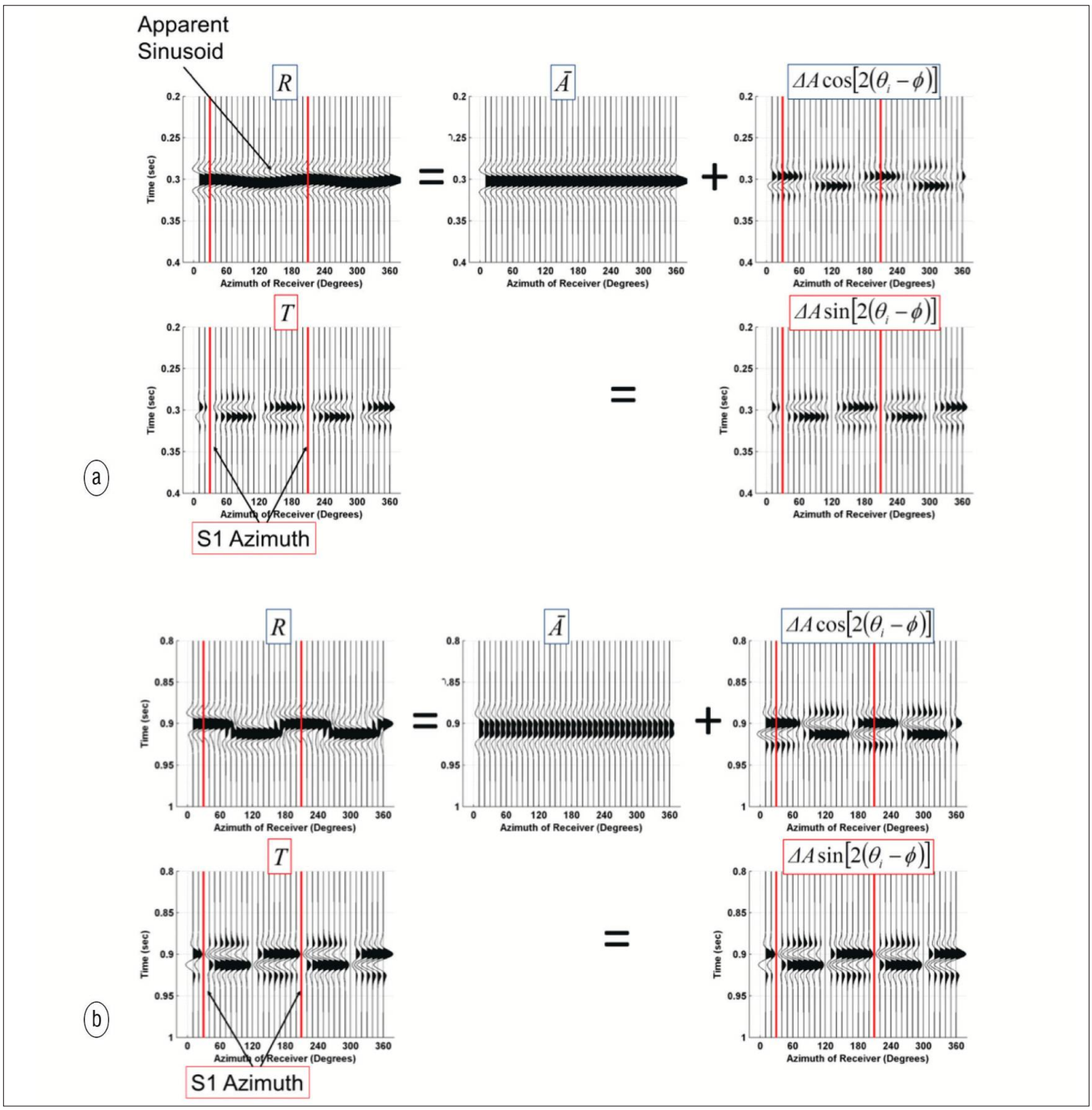

Figure 6. *Illustration of azimuthal amplitude variation for synthetic example. For the shallow event (a), the radial component (top left) appears to have a sinusoidal time variation with azimuth, but in fact this results from the interference between the S1 and S2 modes with different sinusoidal amplitude effects. The radial response can be decomposed into the sum of* Ā*, the average of S1 and S2, and a sinusoidal term proportional to* ΔA*, with* 2θ *variation. Compare this with the transverse which also exhibits the sinusoidal variation but with different phase. For the deeper event (b,) the distinct modes have become more evident on the radial.*

S2 modes (related to the differential term ΔA) rather than an intrinsic time variation. As the time delay increases, we see that this apparent sinusoidal event actually separates into two events with azimuthal amplitude variation (Figure 6b).

The amplitudes of the response can be related to the theory of thin layers as initially expounded by Widess (1973), if it is assumed that S1 and S2 response functions are related simply by Δt, the S1-S2 time delay, as $A_2(t) = A_1(t - \Delta t)$. Then from the Taylor series of calculus, we have, for small Δt

$$\Delta A(t) = \tfrac{1}{2}\left[A_1(t) - A_1(t - \Delta t)\right] \cong \tfrac{1}{2}\Delta t\, dA_1/dt \quad (3)$$

Thus ΔA is proportional in amplitude to Δt, for small amounts of splitting. This amplitude effect can be observed by comparing Figure 6a (lesser Δt) with Figure 6b (greater Δt).

This is all well and good, but do we see this theoretical behavior in real data? Figure 7 shows the same decomposition described above for the radial and transverse data at two different locations from a real heavy-oil data set, with large (7a) and small (7b) amounts of splitting. The example illustrates the same behavior that was observed on the synthetic data, with amplitudes of the radial difference ΔA similar in magnitude to the transverse, and both of them related to the time delay Δt.

S1 orientation analysis using radial and transverse

Shear-wave splitting analysis is often performed as a two-step process: first, estimate the azimuth of the S1 direction and, second, estimate the time-delay between S1 and S2. Typically the transverse component is used to estimate the S1 azimuth, based on the azimuthal position of polarity flips or using an amplitude-fitting approach (Bale et al., 2005). We refer to this as the T-only method.

However, as suggested in the previous section, amplitude information from the radial can also be incorporated in the process. We describe an algorithm to do this, based upon amplitudes as given in Equation 2. This can be written as the equation (see also Bale et al., 2012),

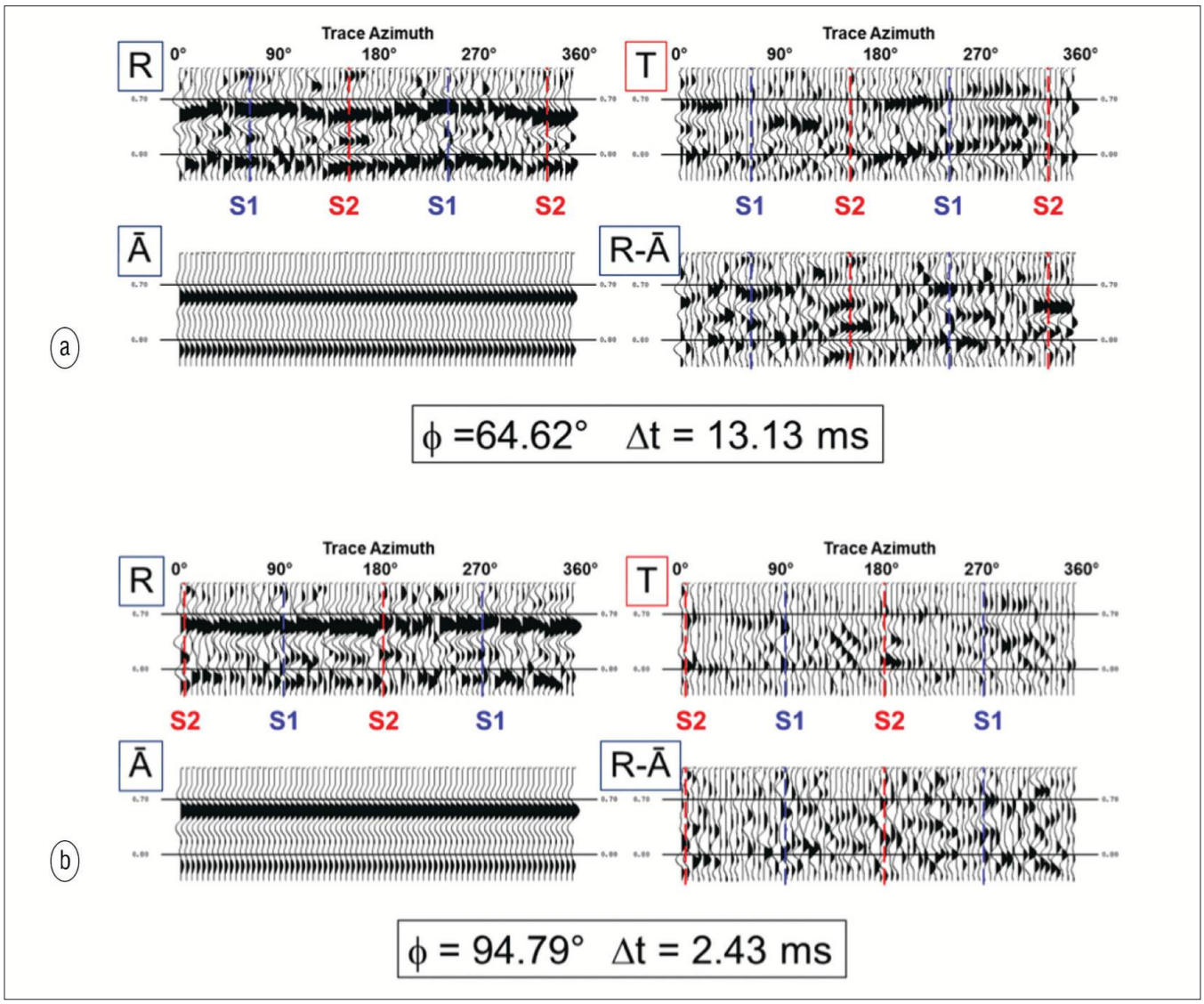

Figure 7. *Real data example of decomposition of radial (R) into average (Ā) and difference (ΔA) terms and comparison with transverse (T), for S1-S2 delay of 13.13 ms (a) and 2.43 ms (b).*

$$\begin{pmatrix} R(t,\theta_i) \\ T(t,\theta_i) \end{pmatrix} = \begin{pmatrix} 1 & \cos(2\theta_i) & \sin(2\theta_i) \\ 0 & \sin(2\theta_i) & -\cos(2\theta_i) \end{pmatrix} \begin{pmatrix} \overline{A}(t) \\ \Delta A(t)\cos(2\varphi) \\ \Delta A(t)\sin(2\varphi) \end{pmatrix}, \quad (4)$$

for $i = 1, \ldots, N$.

If we consider all N equations implied by Equation 4, we get the matrix equation

$$\mathbf{Y} = \mathbf{AX} \quad (5)$$

where

$$\mathbf{Y} = \begin{pmatrix} R(t,\theta_1) \\ \vdots \\ R(t,\theta_N) \\ T(t,\theta_1) \\ \vdots \\ T(t,\theta_N) \end{pmatrix}, \quad \mathbf{X} = \begin{pmatrix} \overline{A}(t) \\ \Delta A(t)\cos(2\phi) \\ \Delta A(t)\sin(2\phi) \end{pmatrix},$$

and

$$\mathbf{A} = \begin{pmatrix} 1 & \cos(2\theta_1) & \sin(2\theta_1) \\ \vdots & \vdots & \vdots \\ 1 & \cos(2\theta_N) & \sin(2\theta_N) \\ 0 & \sin(2\theta_1) & -\cos(2\theta_1) \\ \vdots & \vdots & \vdots \\ 0 & \sin(2\theta_N) & -\cos(2\theta_N) \end{pmatrix},$$

which can be inverted, provided $N \geq 2$, to give the usual least-squares estimate

$$\hat{\mathbf{X}} = \left(\mathbf{A}^T\mathbf{A}\right)^{-1}\mathbf{A}^T\mathbf{Y}. \quad (6)$$

The second and third terms of the solution vector $\hat{\mathbf{X}}$ can then be combined to determine ϕ. We refer to this as the R + T method.

What is the advantage in using both radial and transverse as opposed to transverse alone? As discussed in the previous section, the higher SNR on the radial is of no direct benefit, as it doesn't apply to the part which has azimuthal dependence. However, there is an effective improvement in azimuthal sampling which arises from the different azimuthal dependence of R and T, as shown in Equation 2.

Figure 8 shows a comparison of S1 azimuth estimates measured on a heavy oil data set at the Devonian level (about 1 s PS time) using 5 × 5 and 11 × 11 superbin sizes between T-only and R+T methods. The receiver-line spacing for this survey is 150 m, which causes a noticeable acquisition footprint that contaminates the analysis results for shallow targets. As is seen in Figure 8, for 5 × 5 superbin sizes, the footprint is somewhat reduced using the R+T method compared to the T-only method. However, if the superbin size is increased to 11 × 11, which is necessary to remove the footprint satisfactorily, then both methods perform equally well.

On data which have been acquired more densely (such as the Kerrobert survey in the following section), we did not find a material difference between T only and R+T methods. We conclude that use of the R+T is a tool which is not necessary in many cases, but may be helpful when dealing with coarsely sampled (i.e., line spacing) PS data especially for shallow targets.

Having determined the S1 direction, we next determine the time delay by first applying a rotation to S1 and S2 directions, performing a weighted stack to obtain S1 and S2 traces, and then using a cross-correlation technique. At this point, we have an estimated S1 direction ϕ, and time delay Δt, for each CCP location in the survey, at the current analysis depth.

Layer stripping

Because the Earth may contain layers with different stress or fracture regimes, leading to different S1 directions, the recorded shear waves may have been split multiple times, with both S1 and S2 from the deepest layer being split again into new S1 and S2 directions from the layer above, and so on. This results in considerable complexity of waveform in which the directions for layers are masked by layers above, for all but the shallowest layer. It is important to unravel this effect

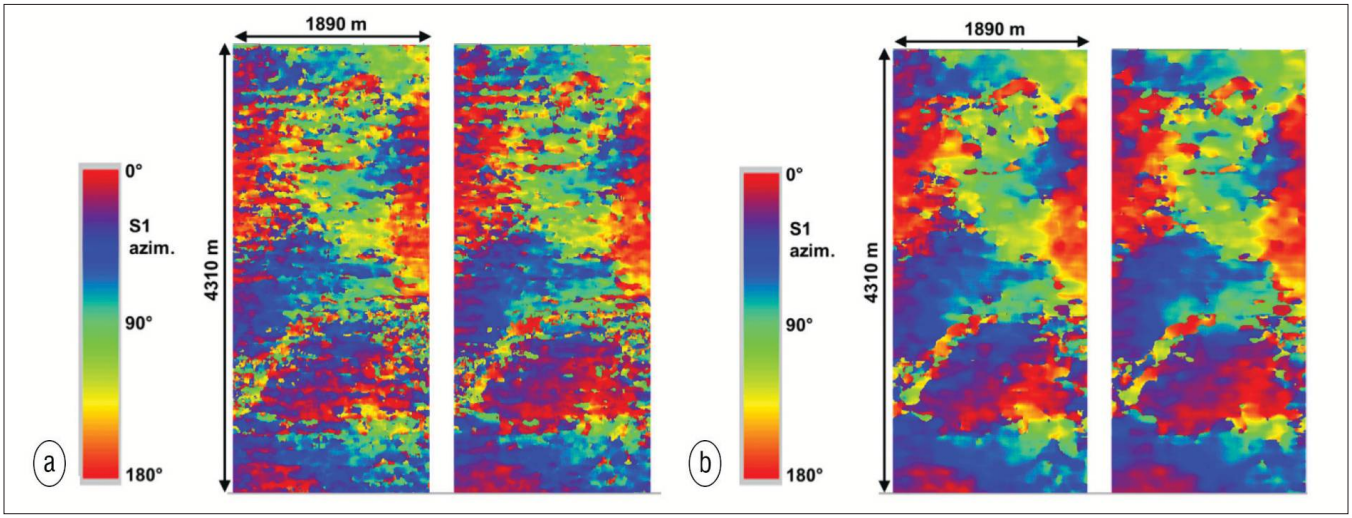

Figure 8. *Comparison of S1 azimuth estimates with superbinned input, using (a) 5 × 5 superbins and (b) 11 × 11 superbins. In each case, transverse-only analysis is shown on the left, and radial + transverse analysis is shown on the right.*

to find the splitting characteristics at the target depth.

To take into account the existence of several different layers with different S1 directions, we perform layer stripping. In each layer-stripping step, the estimated time delay is computed as above, then applied on the data after rotation to S1-S2 coordinates, by first shifting the P-S2 data to match P-S1 and then rotating back to the radial-transverse coordinate system. The resulting data may be referred to as radial-prime and transverse-prime (R' and T'). This procedure is illustrated in Figure 9, using the Kerrobert data set shown later as our case study.

In order to layer strip through multiple layers, it is necessary to compute R' and T' for each layer in succession, in order to perform analysis for the subsequent layer. Usually the R' data set is the most suitable for the final goal of imaging the reservoir, although it is also quite possible to generate P-S1 and P-S2 images after the final layer-stripping step.

Data example: Shear-wave splitting from an in-situ combustion EOR project

In-situ combustion (ISC) processes burn the heavier elements of oil in situ and mobilize the lighter ends for recovery. What matters in our example, though, is that, after the combustion front passes, all that remains is sand with effectively no residual hydrocarbons. In a well consolidated sandstone, we would assume that the effect of this would be purely stress-related, in that the fluid and its support of stresses has disappeared and been replaced by air flowing to the combustion front at a certain pressure. In unconsolidated heavy oil reservoirs, such as Kerrobert or many others in Western Canada, the matrix is often partly made up of oil. In bitumen reservoirs in the Alberta oil sands, the matrix is mostly the oil itself, with sand suspended within it. We must assume then that EOR processes, such as ISC or other thermal methods, can cause matrix deformation or complete reorganization during recovery. In addition to the effect this would have on how the formation carries stresses, this could affect the splitting signature that we are monitoring. To our knowledge, this mechanism of splitting has not been tested in the lab. It must be given consideration, though, because of the physics of the processes being employed for recovery and the unconsolidated formations that they are being used in.

Examples of the application of shear-wave splitting analysis are shown in Figures 10 and 11. In this case, shear-wave splitting analysis over the reservoir interval of an active ISC project highlights the stress and/or matrix change with time as the combustion front progresses. In this specific case, it is known that the operation is well below the fracture pressure of the interval and that the reservoir itself is not known to be fractured from extensive core samples and logging. The implication of this is that the ample amount of splitting observed in the reservoir (7 ms maximum over a 50-ms layer window), after layer stripping of the above layers, is substantial and most likely due to stress and/or matrix changes within the formation from ISC (for more complete information on this example please see Wikel and Kendall, 2012, or Bale et al., 2012).

This type of analysis is useful for gauging the progression of the combustion front along with PP time-lapse data and other reservoir engineering information. It is hoped that this type of analysis can aid in constraining future reservoir simulations for a more accurate representation of what is occurring in the subsurface. In addition, these results open up new areas of study utilizing multicomponent data for monitoring other types of EOR projects in both the overburden for cap-rock integrity and reservoir formations to monitor progression of the process (thermal, polymer, CO_2 injection).

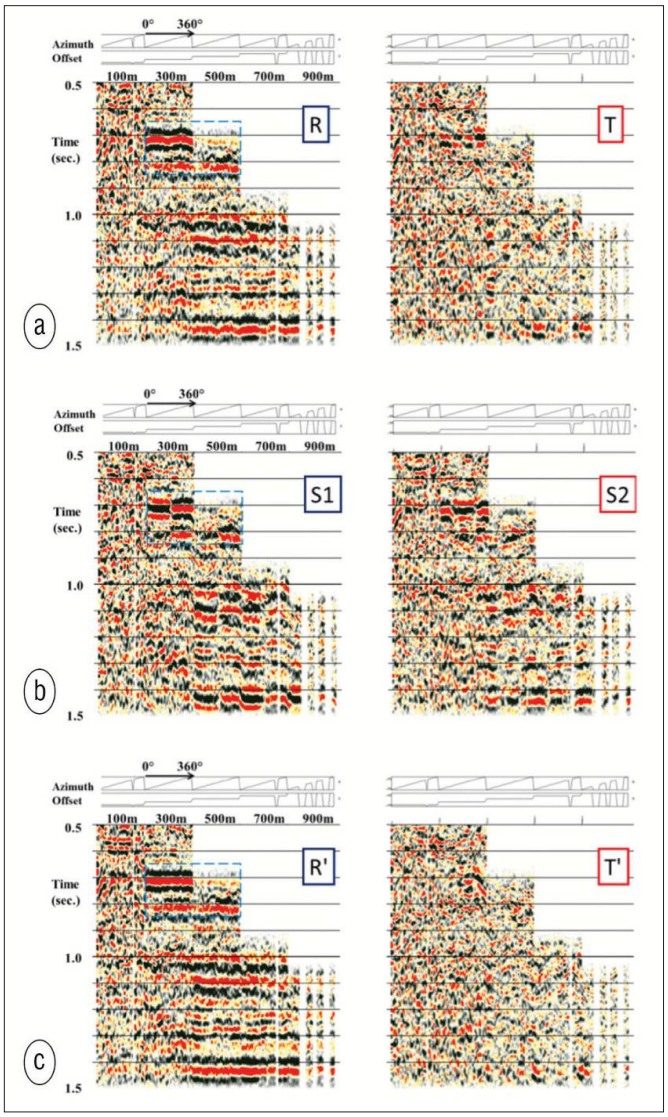

Figure 9. *Illustration of process from original radial and transverse through splitting correction to derive radial and transverse "prime." The input data (a) are shown as common asymptotic conversion point (ACP) gathers where data are indexed first by offset range, and then by shot-receiver azimuth, (see profiles above the gathers). The gathers are superbinned using 7 × 7 bins to improve SNR. The blue dashed box shows the range used for shear-wave splitting analysis. Using the S1 azimuth derived from the analysis, the data are rotated to the coordinate system defined by S1 and S2 directions (b). Using a time delay estimated from the analysis (about 10 ms), the S2 data are shifted upward to align with the S1 data. Finally in (c), the data are rotated back to the R-T coordinate system where the removal of the anisotropy effect is evident. These are referred to as R' and T'.*

Conclusions

The need for more information on the stress changes associated with thermal production of heavy oil reservoirs, both in terms of assuring cap-rock integrity and monitoring the production, has motivated the application of shear-wave splitting from multicomponent data. Shear-wave splitting appears well suited to detection of differential horizontal stress effects. Stress-related splitting has been demonstrated using ultrasonic tests on a sandstone sample, though the exact mechanisms involved within the heavy oil environment are still poorly understood.

The signature of shear-wave splitting when mapped by azimuth is characterized by strong—apparently sinusoidal in time—amplitudes on the radial component, and weaker amplitudes on the transverse, which exhibits polarity reversals. We show that, for the standard models of shear-wave splitting, the radial behavior can be decomposed into an azimuthally invariant part and an azimuthally sensitive part of comparable magnitude to the transverse, but with a different azimuthal phase. Thus the higher signal level of the radial is of no direct benefit for anisotropy analysis, on its own. However, the combination of radial and transverse (R+T) is of some benefit, when applied on data with coarse line sampling. Nevertheless, we still believe superbinning is currently a requirement for most land data splitting analysis.

We applied shear-wave splitting analysis with four layers of layer stripping to obtain measurements of stress in a heavy oil reservoir in Canada. The layers analyzed included a cap-rock layer and the heavy oil layer itself. We observed an anomalously high level of splitting in the vicinity of the

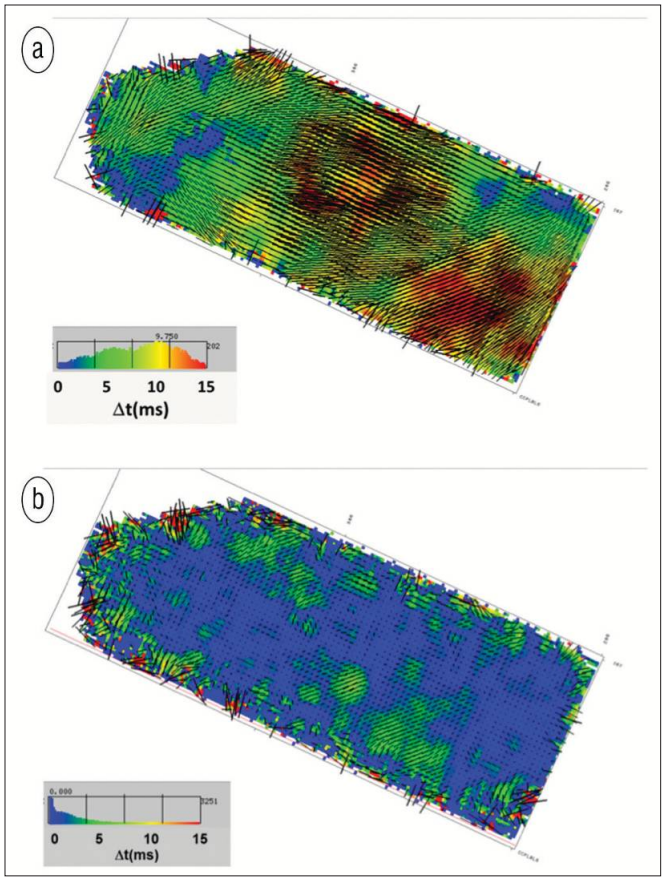

Figure 10. *Overburden (a) and cap-rock (b) analysis for shear-wave splitting. The color underlay represents the time delay between S1 and S2 modes, with a range from 0 to 15 ms, as shown in the histograms. The line segments represent both time delay (length) and S1 azimuth.*

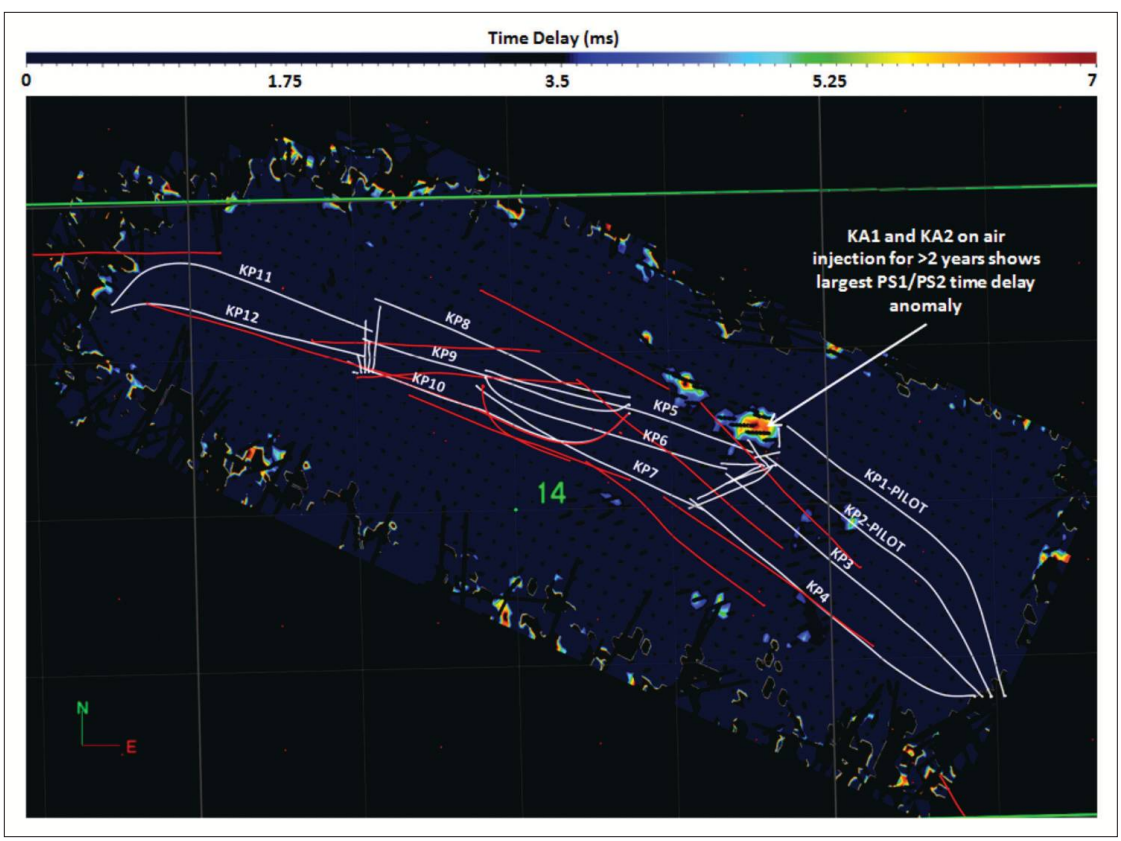

Figure 11. *PS1/PS2 time delay in color with the PS1 direction overlain as a vector scaled by the time delay in October 2011. White wells are ISC development air (directional vertical wells) and production (horizontal wells). KP1 and KP2 were the initial ISC pilot wells that have been injecting air since November 2009. KP3-12 were brought online with air injection in July-August 2011 and are in the start-up stages of ISC. Red wells are legacy primary production wells.*

combustion zone, which we suggest represents a measurement of the stress or possible matrix effect associated with the thermal process. This suggests shear-wave splitting may be an important tool for ongoing monitoring of stress effects, in order to responsibly manage thermal production of heavy oil resources. TLE

References

Bale, R. A., J. Li, B. Mattocks, and S. Ronen, 2005, Robust estimation of fracture directions from 3D converted waves: 75th Annual International Meeting, SEG, Expanded Abstracts, 889–892, http://dx.doi.org/10.1190/1.2148302.

Bale, R, T. Marchand, K. Wilkinson, K. Wikel, and R. Kendall, 2012, Processing 3C heavy oil data for shallow shear-wave splitting properties: Methods and case study: CSEG Recorder, **37**, May.

Cary, P., X. Li, G. Popov, and C. Zhang, 2010, Shear wave splitting in compliant rocks: The Leading Edge, **29**, no. 10, 1278–1285, http://dx.doi.org/10.1190/1.3496918.

Dillen, M. W. P., 2000, Time-lapse seismic monitoring of subsurface stress dynamics: PhD thesis, Delft University.

Gaiser, J. E., P. J. Fowler, and A. R. Jackson, 1997, Challenges for 3D converted-wave processing: 67th Annual International Meeting, SEG, Expanded Abstracts, 1199–1202, http://dx.doi.org/10.1190/1.1885611.

Gumble, J. E., and J. E. Gaiser, 2006, Characterization of layered anisotropic media from prestack PS-wave-reflection data: Geophysics, **71**, no. 5, D171–D182, http://dx.doi.org/10.1190/1.2335419.

Li, X.-Y., 1998, Fracture detection using P-P and P-S waves in multicomponent sea-floor data: 68th Annual International Meeting, SEG, Expanded Abstracts, 2056–2059, http://dx.doi.org/10.1190/1.1820357.

Liu, W., H. Dai, and X.-Y. Li, 2012, The analysis of the azimuthal variation of PS converted waves in HTI media: A synthetic study: 82nd Annual International Meeting, SEG, Expanded Abstracts, doi 10.1190/segam2012-0622.1.

Sayers, C. M., 2010, Geophysics under stress: Geomechanical applications of seismic and borehole acoustic waves: SEG, http://dx.doi.org/10.1190/1.9781560802129.

Simmons, J. L. Jr., 2009, Converted-wave splitting estimation and compensation: Geophysics, **74**, no. 1, D37–D48, http://dx.doi.org/10.1190/1.3036009.

Thomsen, L., I. Tsvankin, and M. C. Mueller, 1999, Coarse-layer stripping of vertically variable azimuthal anisotropy from shear-wave data: Geophysics, **64**, no. 4, 1126–1138, http://dx.doi.org/10.1190/1.1444619.

Whale, R., R. Bale, K. Poplavskii, K. Douglas, X. Li, and C. Slind, 2009, Estimating and compensating for anisotropy observed in PS data for a heavy oil reservoir: 79th Annual International Meeting, SEG, Expanded Abstracts, **28**, 1212–1216http://dx.doi.org/10.1190/1.3255070.

Widess, M., 1973, How thin is a thin bed?: Geophysics, **38**, no. 6, 1176–1180, http://dx.doi.org/10.1190/1.1440403.

Wikel, K., R. Kendall, R. Bale, J. Grossman, and K. DeMeersman, 2012, 4D-3C geomechanical study of in-situ bitumen recovery utilizing toe to heel air injection (THAI®), Alberta, Canada: First Break, **30**, 43–53.

Wikel, K., and R. Kendall, 2012, 4D study of secondary recovery utilizing THAI® from a Saskatchewan heavy oil reservoir: 2012 CSEG GeoConvention, Expanded Abstracts.

Acknowledgments: We thank Key Seismic Solutions and Petrobank Energy and Resources for permission to publish this work. We also thank Jeff Deere, Jim Gaiser, and Rishi Bansal for their careful reviews and helpful suggestions.

Corresponding author: Richard.Bale@keyseismic.com